AIAA JOURNAL
Vol. 37, No. 5, May 1999

Development and Validation of Navier–Stokes Procedure for Turbomachinery Unsteady Flow

A. Chernobrovkin* and B. Lakshminarayana†
Pennsylvania State University, University Park, Pennsylvania 16802

An unsteady viscous flow solver based on the Runge–Kutta scheme has been developed. Three low-Reynolds-number k-ε turbulence models have been assessed for their ability to predict unsteady transitional flow. The k-ε model has been modified to incorporate leading-edge effects. A pseudo time approach has been used to accelerate the numerical algorithm for unsteady flows. A sensitivity study has been carried out, including the effects of the artificial dissipation, the grid density, and the physical and pseudo time steps. The numerical simulation of the unsteady transitional flow in a compressor cascade has been carried out successfully. Good agreement with the measured data as well as the previous Euler/boundary-layer predictions has been achieved. The numerical solver has been able to predict major features, associated with the wake-induced transition on a compressor blade (wake-induced transitional strip, wake-induced turbulent strip, etc.). An analysis and an interpretation of the results from the unsteady flow simulation have been carried out to understand additional flow physics associated with the transitional flow.

Nomenclature

A	= wake amplitude, $A = (U_f - U_c)/U_f$
Am[]	= amplitude of the first harmonic
C	= chord length
C_f	= skin friction coefficient, $\tau_w/(\rho U_0^2)$
C_p	= pressure coefficient, $C_p = (p - p_0)/(\rho U_0^2/2)$
C_x	= axial chord length
c_μ, $c_{\varepsilon 1}$, $c_{\varepsilon 2}$	= constants in low-Reynolds-number turbulence models
G, g	= amplification factor
$\tilde{g}_{k_1 k_2}$	= average amplification factor: $\tilde{g}_{k_1 k_2} = \int_{k_1}^{k_2} \frac{g(k)\,\mathrm{d}k}{(k_2 - k_1)}$
H	= shape factor
k	= turbulent kinetic energy wave number
k_4	= coefficient of the fourth-order artificial dissipation
M	= Mach number
n	= number of grid points per wave length
P	= turbulent kinetic energy production
Ph[]	= phase of the first harmonic
p	= static pressure
Q	= vector of conservative variables
R	= residual
R_{ij}	= rotation-rate tensor
Re	= Reynolds number, based on chord
Re_t	= turbulent Reynolds number, $k^2/\nu\varepsilon$
Re_y	= turbulent Reynolds number, $\sqrt{(k)}y/\nu$
Re_θ, Re_x	= Reynolds number, based on θ, x
$\hat{S}^k$	= numerical discretization of the physical time derivatives at k stage of the Runge–Kutta scheme
S_{ij}	= strain-rate tensor
T	= period
T_u	= turbulence intensity
t	= physical time
U	= total velocity
u_τ	= friction velocity, $\sqrt{(\tau_w)/\rho}$
V_{0w}	= wave velocity in y direction (rotational velocity)
v	= y component of velocity
x	= axial length measured from leading edge
x_c	= chordwise distance measured from leading edge
y	= distance in circumferential direction
y^+	= inner variable, $u_\tau y/\nu$
α_k	= coefficient of Runge–Kutta scheme
α'_k, α''_k	= coefficient of Runge–Kutta scheme with pseudo-time stepping [Eq. (1)]
β	= inlet flow angle
Δ	= difference between maximum and minimum values during the period
δ	= $\Delta\tau/\Delta t$
ε	= turbulence dissipation rate
θ	= momentum thickness
λ	= Courant–Friedrichs–Lewy number
μ_t	= eddy viscosity coefficient
ν	= molecular viscosity
σ	= Von Neuman number
τ	= pseudo time
Ω	= reduced frequency, $\Omega = \varpi C_x/U_0$
ω	= wake width parameter
ϖ	= wake passing frequency

Subscripts and Superscripts

c	= values at the wake centerline
e	= values at the edge of the boundary layer
f	= values in the freestream
ref	= reference value
t	= turbulent
t_e	= trailing edge
w	= quantity at the wall
0	= total, inlet, freestream
$^-$, aver	= time average

Presented as Paper 97-3281 at the AIAA/ASME/SAE/ASEE 33rd Joint Propulsion Conference, Seattle, WA, July 6–9, 1997; received Aug. 26, 1997; revision received Aug. 25, 1998; accepted for publication Jan. 2, 1999. Copyright © 1999 by A. Chernobrovkin and B. Lakshminarayana. Published by the American Institute of Aeronautics and Astronautics, Inc., with permission.

*Graduate Research Assistant, Center for Gas Turbines and Power.
†Evan Pugh Professor of Aerospace Engineering and Director, Center for Gas Turbines and Power. Fellow AIAA.

Introduction

THE unsteady flow in turbomachines because of rotor-stator interaction results in blade vibration, noise generation, decreased durability, and penalty in aerodynamic performance. An understanding of the physics of the unsteady flow and the development of predictive capabilities is essential for improved overall performance, durability, and reliability. Transition associated with the unsteady flow is an extremely complex phenomenon and its understanding can lead to improved efficiency, decreased losses, and improved cooling for turbines. Some attempts have been made to analyze

the ability of the computational fluid dynamics code to predict the unsteady transitional flow. Fan and Lakshminarayana[1] modified the k-ε model to capture near-wall physics of the unsteady flow. This model was incorporated in a coupled Euler/boundary-layer procedure to develop an efficient and accurate tool for the simulation of the unsteady transition induced by a moving wake. The need to model more complex and off-design cases as well as high-speed flow requires the development of a Navier–Stokes procedure to overcome the limitation of the inviscid/parabolic approach.

Even though some attempts have been made to develop and use unsteady Navier–Stokes solvers for prediction of rotor-stator interaction effects, none have been validated satisfactorily against accuracy, especially for its ability to capture the unsteady transitional viscous layers near blade and wall surfaces. This is the object of the research reported in this paper.

Numerical Procedure

The flow solver is based on the full, Favre-averaged, Navier–Stokes equations. An explicit four-stage Runge–Kutta scheme is used for the time integration of both mean-flow and turbulence equations. A compact second-order accurate central difference flux evaluation scheme is employed for convection terms. Diffusion terms are discretized using second-order accurate central differences. A detailed description of the numerical procedure for the steady solver can be found in Ref. 2. Numerical simulation of the unsteady flow requires special treatment to reduce possible reflections at the boundaries. One- and two-dimensional, Giles-type, nonreflecting boundary conditions are incorporated to minimize the reflection at boundaries and correspondingly to minimize the computational domain. A number of low-Reynolds-number k-ε turbulence models—Chien,[3] denoted as CH, Lam and Bremhorst,[4] denoted as LB, and Fan et al.,[5] denoted as FLB—are utilized for turbulence closure.

The steady Navier–Stokes solver developed earlier[2] has been modified by the authors to enable time-accurate simulations. Even if a time-marching scheme is used to approximate unsteady equations, discretization errors and acceleration techniques can destroy the time accuracy of the code. Time-accurate computations require that the amplitude of $G = Q^{n+1}/Q^n$ be close to one for all harmonics to be resolved. Also, phase-angle error has a major influence on the time accuracy. Thus special care should be taken in applying time-marching schemes, developed for the steady-state calculation, for the unsteady numerical simulation. This special case includes additional restrictions on the time step, i.e., the time step should be constant for all cells. When an explicit time-marching code is used for the unsteady computation, the time step is limited by the stability considerations. Because of this limitation, the actual time step is much smaller than the time step required for the temporal accuracy, especially in the case of highly stretched grids in viscous regions. Furthermore, it is impossible to use common acceleration techniques, such as the multigrid and the implicit residual smoothing. These techniques generally affect the temporal accuracy of computations. These limitations lead to a large increase in CPU time for unsteady viscous computations on highly stretched grids. These difficulties can be overcome by the implementation of internal iterations at each time step. The base code has been extended to include the pseudo time inner iteration. This approach resulted in a major acceleration of the unsteady code. Details of the pseudo time scheme incorporated in this paper are discussed in the following.

The code has been calibrated using exact analytical solutions (e.g., flow over a cylinder, flat-plate laminar boundary layer, oscillating plate, etc.) validated against benchmark quality data (e.g., unsteady turbulent boundary layer, transition over a flat plate, etc.) and certified for complex flows (compressor and turbine rotors, turn around duct, etc.). Based on previous steady-flow analysis, numerical uncertainty of the code for the velocity field (i.e., error due to the discretization, computer round off, etc.) is estimated to be less than 3% (maximum error) and 0.5% (rms error). To achieve this level of accuracy, proper numerical strategy should be carried out (i.e., grid dependency analysis, adequate level of iterative convergence, etc.). Additional factors affecting numerical uncertainty of the code in the case of unsteady-flow problems are discussed next.

Different approaches have been used in the discretization of the physical derivative in pseudo time step techniques. These approaches for the discretization of the equation $\partial Q/\partial t = R$ can be expressed as follows:

$$[1 + \alpha'_k(\Delta\tau/\Delta t)c]\Delta Q^k = -\alpha_k \Delta\tau(\hat{S}^{k-1} + \hat{R}^{k-1}) + \alpha''_k(\Delta\tau/\Delta t)c\Delta Q^{k-1} \tag{1}$$

Second-order accurate discretization of the time derivatives can be written as

$$\frac{\partial Q}{\partial t} = \hat{S} = \frac{3Q^{k-1} - 4Q^n + Q^{n-1}}{2\Delta t}$$

in this case $c = \frac{2}{3}$. Values of α'_k, α''_k, the coefficients used by various authors, are given next: 1) $\alpha'_k = 0$, $\alpha''_k = 0$—explicit treatment of physical derivatives in internal cycle[6]; 2) $\alpha'_k = 1$, $\alpha''_k = 0$—implicit discretization of physical derivatives[7]; 3) $\alpha'_k = \alpha_k$, $\alpha''_k = \alpha_k$—also implicit discretization of physical derivatives[8]; and 4) $\alpha'_k = \alpha_k$, $\alpha''_k = 0$.

The presence of the additional source term in Eq. (1) changes the behavior of the scheme. Melson et al.[8] carried out Von Neuman stability analysis of a five-stage Runge–Kutta scheme. This analysis has been applied to the four-stage scheme and has been extended to include different cases already described. The following two-dimensional model equation has been utilized for this analysis:

$$\frac{du}{d\tau} + \frac{du}{dt} + a\frac{du}{dx} + b\frac{du}{dy} = \upsilon\left(\frac{d^2u}{dx^2} + \frac{d^2u}{dy^2}\right) + k_4\left(a\Delta x^3\frac{d^4u}{dx^4} + b\Delta y^3\frac{d^4u}{dy^4}\right) \tag{2}$$

where $\alpha_1 = \frac{1}{4}$, $\alpha_2 = \frac{1}{3}$, $\alpha_3 = \frac{1}{2}$, and $\alpha_4 = 1$.

A numerical scheme with evaluation of all terms at all stages (denoted as 1, etc.) as well as schemes with the evaluation of source and viscous terms only at the first stage (denoted as 1a, etc.) were considered. An amplification factor of $g = g(\lambda_x, \lambda_y, \sigma_x, \sigma_y, \sigma'_x, \sigma'_y, \delta, k_x, k_y)$ was derived using the symbolic computation program Mathematica. Only one-dimensional results are presented here for the sake of clarity. The second dimension does not principally alter the results but makes the evaluation and interpretation more difficult.

The ratio of the pseudo time step to the physical time step, $\delta = \Delta\tau/\Delta t$, plays a significant role in the behavior of the scheme. The results of the stability analysis for the scheme 1a are presented in Fig. 1. An average amplification factor of $\tilde{g}_{0\pi/2}$ is plotted as a function of the Courant–Friedrichs–Lewy number, Von Neuman number, and δ. The plot is bounded by the stability surface with $|g| = 1$. Explicit discretization of the physical derivatives leads to a linear decrease in the maximum Von Neuman number with increasing δ. On the contrary, an implicit evaluation of the physical time derivatives leads to an extended stability region. An extended stability region indicates an advantage of the implicit evaluation of the physical temporal derivatives. However, the distribution of $\tilde{g}_{0\pi/2}$ suggests that within the stability region a scheme with an explicit evaluation of the physical time derivatives may have better convergence. With increasing δ, the average amplification factor $\tilde{g}_{0\pi/2}$ is smaller for this scheme. The presence of the additional term results in a smaller amplification factor at low wave numbers for both variants of discretization, which is especially beneficial for the calculation of the wake propagation in turbomachinery configurations in which initial error at each physical step predominately consists of the same harmonics as the inlet disturbance, with wave numbers $<\pi/2$. Thus, the low amplification factor for these wave numbers may accelerate an overall convergence. More details of the stability analysis can be found in Ref. 9. Based on the stability analysis, operational curves were established for both schemes. These curves are used to adjust time step according to local value of δ for both the explicit and the implicit discretization of temporal derivatives.

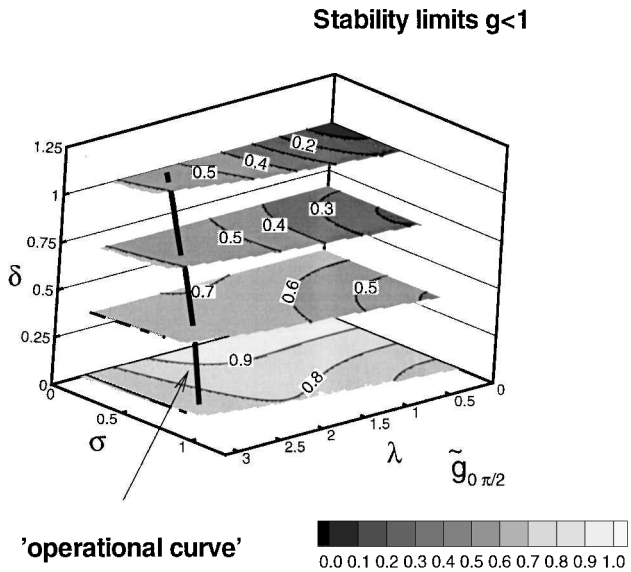

Fig. 1 Stability limits and $\tilde{g}_{0,\pi/2}$ distribution for the scheme with implicit evaluation of the source term.

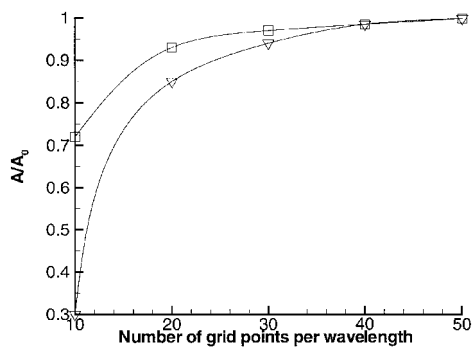

Fig. 2 Wake decay due to the artificial dissipation; propagation length is equal to six wavelengths: □, $k_4 = 0.005$, and ▽, $k_4 = 0.02$.

Code Validation

One of the objectives of this research is to assess the accuracy of the unsteady flow code against the experimental data and the predictions from a boundary-layer code. This objective is carried out in several steps outlined in the following.

Influence of the Artificial Dissipation on the Wake Propagation

Inviscid numerical simulations were carried out to determine the influence of the artificial dissipation and outlet boundary conditions on the unsteady wake decay. Unsteadiness was prescribed through a moving sinusoidal wake at the inlet. Results of the numerical simulation are shown in Fig. 2. For typical values of the fourth-order artificial dissipation coefficient k_4, 20–30 grid points per each wave width are necessary for accurate prediction. The results of this analysis are used as a guideline in generating grids for additional test cases. One of the cases is a development of the wake downstream of the flat plate measured by Chevray and Kovasznay.[10] The prediction is in a good correlation with the data.

Transitional Flow on a Flat Plate

The numerical simulation of the transitional flow on a flat plate was carried out to assess the ability of the code to predict the inception and the length of the transition. The test case chosen for this validation is T3a described by Savill.[11] The predictions from all three turbulence models (CH, LB, FLB) are compared with the data.

The skin friction coefficient distribution, shown in Fig. 3, indicates that the LB model shows the best agreement with data for low turbulence intensity, whereas the CH model predicts very premature transition and the longest transitional length. The numerical simulation of the flat-plate flow with higher inlet turbulence intensity,

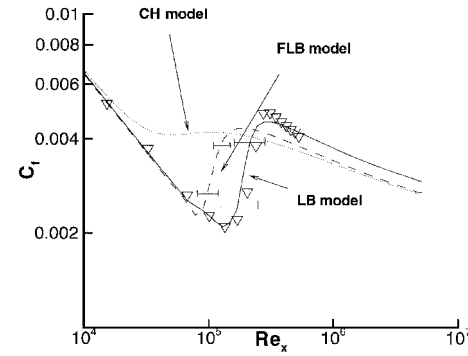

Fig. 3 Simulated steady transition on a flat plate: ▽, experiment T3a, Tu = 3%; ——, modification range due to the variation of k_4 = {0.03–0.005}, artificial dissipation anisotropy coefficient {0, 1}, grid spacing {h – 4h}.

more typical for turbomachinery applications, shows that the LB model gives earlier transition, whereas the FLB model is in a better agreement with the data. This observation can be explained by the fact that the LB model is numerically less stable than the FLB model. The momentum Reynolds number at the start and at the end of the transition, predicted from the Navier–Stokes code, was compared with the correlation of Abu-Ghannam and Shaw[12] and the boundary-layer prediction.[1] The time-marching code predicts earlier inception of the transition at low values of turbulent intensity. Overall, the transition prediction by the Navier–Stokes code is close to the prediction by the boundary-layer code based on the same turbulence model.[9]

Modification of the Turbulence Model for Leading-Edge Flow

The modification of the turbulence near the leading edge of the blade can influence the development of the turbulent boundary layer along the blade. Large flow turning and curvature effects, present in these leading-edge flows, influence the development of the flow near the stagnation point. The experimental data on this effect are scarce. The k-ε turbulence model predicts excessive production of the turbulent kinetic energy and the eddy viscosity in this region. As a result, the boundary layer becomes fully turbulent with a transition occurring very close to the leading edge.

Modification of the k-ε model to improve the accuracy has been suggested by many investigators. The first group of modifications suggested consists of change in the production term. Launder and Spalding[13] suggested the use of the rotation-rate tensor to modify the production term $P = 2\nu_t\sqrt{[(S_{ij})^2 \cdot (R_{ij})^2]}$. Flow near the stagnation point is nearly irrotational, while in the shear layer $\sqrt{[(S_{ij})^2 \cdot (R_{ij})^2]}$ and $S_{ij} \cdot S_{ij}$ are practically equal. This modification reduces the production of turbulence only near the stagnation point while the boundary layer is not affected. In the second approach the dissipation-rate equation is modified. The derivation of this equation is based on numerous assumptions. Strahle et al.[14] suggested setting $C_{\varepsilon 1} = C_{\varepsilon 2}$ (constants in the source term of the ε equation) near the stagnation point in the turbulence energy dissipation equation.

Viscous flow in the compressor cascade, described in the next section, has been simulated using these modifications to the FLB k-ε model for the leading-edge flow. Modifications improve the distribution of the turbulent kinetic energy and enable a reasonably good prediction of the transition. The predicted transition zone is located from 33% of chord to 50% (this correlates well with the experimental data), with a 5% variation between various modifications. Because of a lack of experimental data on the budget of the turbulent kinetic energy along the stagnation line, it is difficult to assess various modifications suggested. The approaches based on the modification of the ε-equation and the modification of the production term suggested by Launder and Spalding[13] were implemented in the simulation of the unsteady transition described next, and these were found to be crucial for the accurate prediction of the unsteady transitional flow.

Numerical Simulation of the Unsteady Flow in a Compressor Cascade

Fan and Lakshminarayana[1] used an unsteady inviscid two-dimensional code coupled with an unsteady boundary-layer code

Table 1 Cascade parameters

Characteristics	Value
Pitch/chord	0.78
Steady inflow angle α	44.2 deg
Re	4×10^6
Reduced frequency Ω	6.12
Wake velocity defect A_0	28.3%
Stagger angle	29 deg
Inlet M	0.299
Wake inflow angle	15.55 deg
Wake width parameter ω	0.095
Variation of the turbulence intensity, ΔT_{u0}	8%

to predict the unsteady flow caused by the transport of a simulated upstream rotor wake through an annular compressor cascade and compared the prediction with the data from Schulz et al.[15] The simulated rotor wake was generated using a rotor consisting of rotating rods. The annular cascade had 24 untwisted blades. Characteristics of the cascade are given in Table 1. According to Schulz et al.,[15] the accuracy of experimental mean pressure and mean velocity measurements is equal to 1.4%.

In the numerical simulation the inlet wake was prescribed as a Gaussian distribution; this was found to be a good approximation of the measured wake. A similar distribution was used to prescribe inlet distribution of the turbulence characteristics. Amplitude and width were adjusted according to experimental parameters:

$$U = U_0 + A_0 \exp\left[-\frac{(y - V_{0w}t)^2}{2\omega^2}\right]$$

$$T_u = T_{u0} + \Delta T_{u0} \exp\left[-\frac{(y - V_{0w}t)^2}{2\omega^2}\right]$$

To assess the accuracy of the code, the predictions based on the Navier–Stokes procedure are compared with the data and with the predictions from the Euler/boundary-layer approach. In some instances, the comparison is done only with the Euler/boundary-layer prediction, because of a lack of the experimental data. The cascade with 44.2-deg inlet flow angles was chosen for numerical simulations.

Sensitivity Studies

Flow simulations were performed using three different grids, 179×61, 189×95, and 201×193, to investigate the grid dependency. The distance between the first grid point and the wall varied from $y^+ = 1.6$ for the coarse grid to $y^+ = 0.6$ for the fine grid. Numerical simulation of the steady flow (C_p and C_f distributions) did not show any significant difference between predictions with 201×193 and 189×95 grids. Numerical simulation of unsteady flows imposes additional requirements on the grid generation. The grid should be fine enough to allow a correct propagation and decay of the unsteady wake through the passage. The numerical analysis presented earlier was used to satisfy this requirement. Fourier decomposition of the inlet wake showed that it has five essential harmonics (based on blade passing frequency). Amplitude of the fifth harmonic is found to be only 1.3% of amplitude of the first harmonic. The grid with 193 grid points in the y direction enables the wake to propagate through the cascade without nonphysical decay caused by numerical factors. In the case of 95 grid points in the y direction, only the fifth harmonic is affected by the artificial dissipation. This effect can be neglected because the fifth harmonic is dispersed rapidly by the physical dissipation. As a result of the grid dependency analysis, a 189×95 grid was chosen in all computations.

The choice of the number of physical time steps per period and the number of inner iterations at each physical time step is an additional factor that affects the accuracy of the unsteady flow simulation. An increase in the number of physical time steps leads to a growth in the temporal accuracy and reduced phase errors. The main requirement is that the physical time step should be small enough to resolve the smallest time scales. Previous research indicated that about 500 physical time steps per period are required for the accurate solution

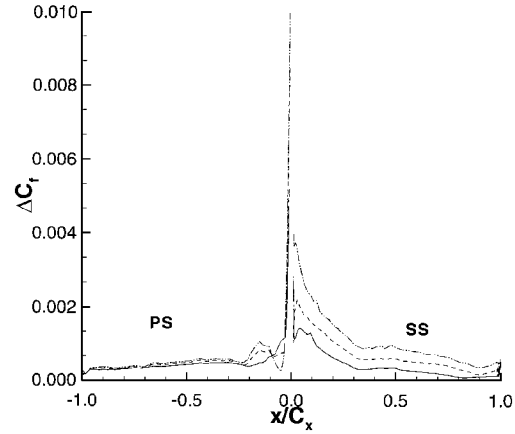

Fig. 4 Influence of the number of inner iterations on the amplitude of the skin-friction coefficient: ——, 10 iterations; – – – –, 20 iterations; – · · – · · –, 50 iterations; PS, pressure surface; and SS, suction surface.

of the wake-blade interaction effect. An increase in the number of physical time steps also affects the number of inner iterations because of the smaller initial error. The change in the number of physical time steps modifies the convergence characteristic of the scheme with a pseudo time stepping. For the case when $\Delta t \to \infty$ (steady-state solution), the additional source term vanishes because of the presence of the physical time derivative. Additional damping at low wave numbers disappears and, correspondingly, convergence of the inner cycle in the freestream slows down. To analyze the effect of the number of physical and inner iterations on the accuracy of the numerical results, a number of numerical tests were carried out.

Numerical simulations were performed with 500 physical time steps and 10, 20, and 50 inner iterations. A comparison of the predicted amplitude of the first harmonic of the unsteady pressure (ΔC_p) on the blade showed no significant difference between 20 and 50 inner iterations. Similar results were obtained for other harmonics and phase angles. On the other hand (Fig. 4), there is a significant change in the amplitude of the C_f variation on the suction surface when the number of inner iterations is increased to 50. Additional numerical experiments showed that a further increase in the number of inner iterations does not affect the accuracy of unsteady C_f distribution. The convergence of the unsteady pressure depends on the convergence characteristics of the numerical scheme in the freestream. The ratio of the pseudo time step to the physical time step is high outside the boundary layer. As a result, additional damping of the low-wave-number harmonics provides very rapid convergence of the unsteady freestream flow. During the first 10 iterations, inner cycle convergence is equal to an analytical value based on the freestream $\Delta\tau/\Delta t$ ratio. This fact also supports the previous conclusion. On the contrary, the correct prediction of the unsteady C_f requires an accurate simulation of the unsteady velocity in the boundary layer. In addition to employing smaller inner steps due to the fine grid, there is no positive effect of the source term in this region ($\Delta\tau/\Delta t \sim 0$). Thus the prediction of the unsteady velocity requires more inner iterations.

Numerical simulations with 250, 500, and 1000 physical time steps were carried out to estimate the influence of the number of physical time steps. The number of inner iterations was 20 for all cases. According to the preceding analysis, this number is sufficient to achieve a converged pressure field. The comparison, presented in Ref. 9, indicates that at least 500 steps are required for the accurate prediction.

Unsteady Pressure Field

The predicted pressure distribution and the unsteady pressure envelope on the blade are shown in Fig. 5. The time-averaged blade-pressure distribution from the Navier–Stokes code is more accurate than the prediction from the Euler code and is also in good agreement with the experimental data because of the presence of the separated region at about 90–95% of the chord. The predicted time

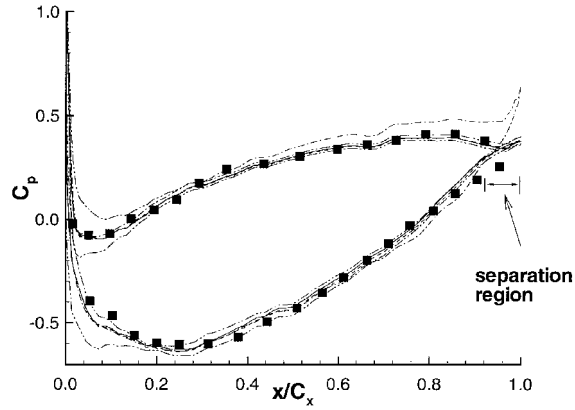

Fig. 5 Blade-pressure distribution: ——, viscous steady; – – – –, viscous, time average; – · · – · · –, viscous min/max; – · – · –, inviscid, steady; and ■, experiment.

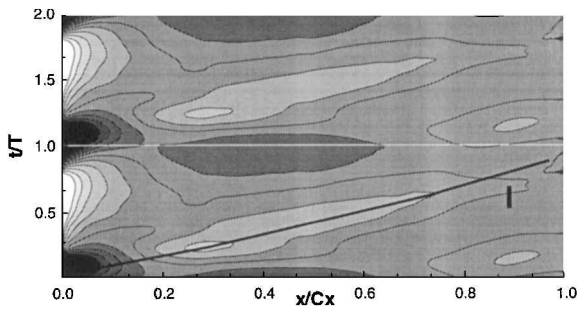

a) Navier–Stokes simulation

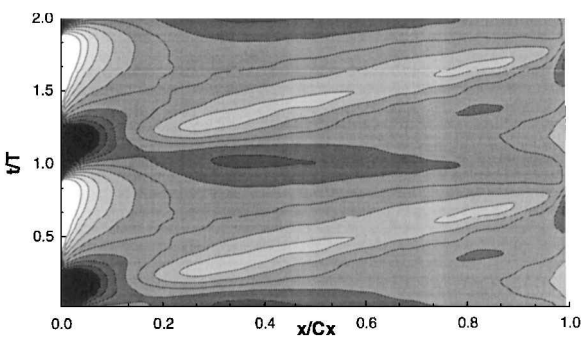

b) Euler/boundary layer simulation

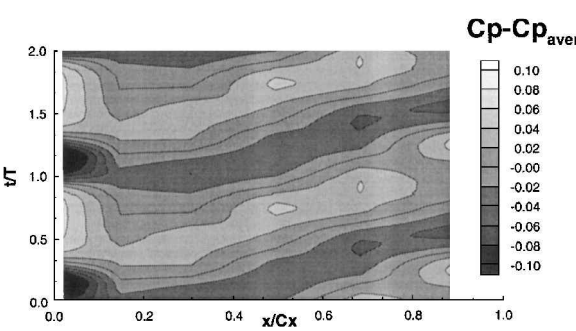

c) Experiment

Fig. 6 Unsteady-pressure distribution: suction surface.

history of the unsteady pressure is compared with the experimental data in Fig. 6. There is a good agreement between predictions and the experimental data. Numerical simulation correctly predicts the maximum unsteadiness near the leading edge where the wake hits the blade; this is caused by a change in the incidence angle and chopping of the wake by the blade. Beyond 20% of the chord, development of the recirculating flow pattern, induced by the passing wake, plays a dominant role in the development of the unsteady pressure, which leads to the region of increased instantaneous pressure along the wake path. Figure 6 indicates that unsteady pressures are predicted well up to 20% of the chord, which is the most important and crucial part of the blade. Both the Euler and the Navier–Stokes code predict smaller pressure variation in comparison with the experimental data, especially from $x/Cx = 60\%$ to 80% on the suction surface. This discrepancy is because of three-dimensional effects in the annular cascade. Flow visualization[15] showed a strong corner separation. Interaction between the upstream wake and the corner separation leads to an amplification of the pressure oscillations. As expected, the Navier–Stokes solution predicts a smaller amplitude in the unsteady pressure at the midchord in comparison with the Euler prediction due to the wake decay caused by the physical dissipation. There is a region of increased unsteadiness in pressure near the trailing edge because of the interaction between the passing wake and the separated region near the trailing edge.

The development of the unsteady pressure field can be explained on the basis of two main mechanisms: wake cutting by the leading edge with associated modification of the incidence angle and development of the recirculating pattern due to the passing wake. Both phenomena are predominantly inviscid. As a result, both the Euler and the Navier–Stokes code predict nearly identical unsteady pressure fields.

Development of the Unsteady Transitional Flow

None of the Navier–Stokes procedures have been validated for their ability to predict the unsteady transitional flow. Numerical simulations have been carried out using three low Re k-ε models: CH, FLB, and LB. The leading-edge modification to the k-ε models, described earlier, was found to be crucial for correct prediction of the transitional flow. Despite the modifications for the leading-edge effect, calculation with the CH model predicts fully turbulent flow all along the blade. Hence, the numerical simulation based on the CH model is not presented in this paper.

In the boundary-layer solution[1] the transitional region extends from $x/C_x = 0.1$ to 0.30. An examination of the skin-friction coefficient distribution in conjunction with the turbulence field shows that the Navier–Stokes code with the FLB model predicts transition from $x/C_x = 0.12$ to 0.4, whereas the computation based on the LB model predicts transition from $x/C_x = 0.1$ to 0.3. An understanding of the complex transitional process on the suction surface can be obtained from a study of the time history of the skin-friction coefficient presented in Fig. 7.

Amplification and modification of the wake and turbulence because of its interaction with the leading edge affects the development of the transitional process. In Fig. 7 path I corresponds to the upstream wake propagation at the edge of the boundary layer, based on the maximum wake defect at that location. Path II (Fig. 7) is the location of the maximum velocity fluctuations in the boundary layer. Beyond 20% of chord, an increase in phase lag between the convection velocity in the boundary layer and in the freestream is observed. An interesting phenomenon takes place in zone A (Fig. 7) along path II. At $t/T = 0$ the wake is located at the leading edge (path I). Change in the incidence angle seriously affects the pressure distribution near the leading edge of the suction surface. As a result of this interaction, a zone with a reduced velocity is generated from 5 to 15% of the chord above the suction surface. This region modifies the development of the boundary layer. A zone of low mean flow is located near the leading edge from about $t/T = -0.1$ to 0.15 and disappears after the passing of the wake. This phenomenon accounts for the difference in the location of the minimum C_f predicted by the Navier–Stokes and the boundary-layer code. Following the classification suggested in Ref. 16, identifying various regions associated with the wake-induced transitional flow is possible. In Fig. 7, A is the region of the wake-induced transition. Disturbance from the wake-boundary interaction leads to an earlier transition. The region B is a region with a transition between wakes and a zone with some features associated with the becalmed region. This region is located downstream of the small, fully laminar zone L. There is a smooth decrease in the shape factor H in zone B (line Z, Fig. 8), whereas in the region of the wake-induced transition, a sharp drop

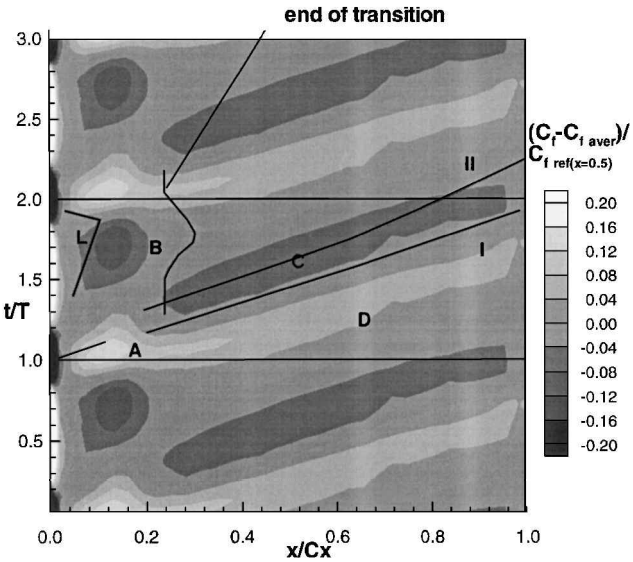

Fig. 7 Skin-friction coefficient: full Navier–Stokes simulation, FLB model.

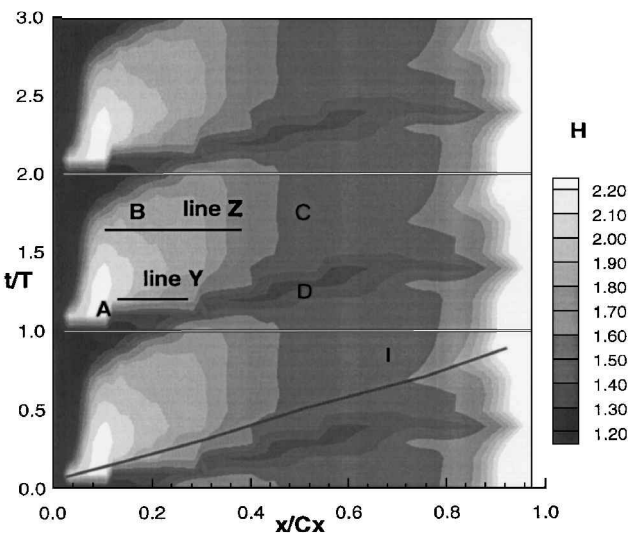

Fig. 8 Shape factor: Navier–Stokes simulation, FLB turbulence model.

of H (line Y) indicates an abrupt transition from the laminar to the turbulent flow. A comparison between predictions based on the FLB model and the LB model shows that the LB model predicts early transition. Zone C is the wake-induced turbulence strip. Two counter-rotating vortices inside the boundary layer, generated by the interaction of the upstream wake with the cascade flow, have a major influence on the unsteady boundary layer downstream of the transitional region. A clockwise rotating vortex near the leading edge of the wake leads to a smaller C_f in the region C. The skin-friction coefficient in the region D (trailing edge of the wake) has increased the level of C_f as a result of the counterclockwise vortex. Boundary-layer simulation predicts no change in the skin-friction coefficient in this region.[1] The Navier–Stokes simulation provides more accurate simulation of the wake behavior in the outer region of the boundary layer and predicts the extended region of this counterclockwise vortex (about 20% of chord). Because of the presence of this vortex, the boundary-layer profile has larger gradients near the wall resulting in increased shear stresses between the wakes.

The transitional flow and the unsteady boundary development are controlled by both the mean velocity defect and turbulence variation in the wake. These two factors have a dissimilar influence in different regions. Unsteady interaction between the mean flow and the turbulence field, with a phase lag between the velocity, the pressure, and the turbulence quantities, make the flow very complex. It is possible to estimate the importance of these two mechanisms from an analysis of the unsteady flowfield simulated by the Navier–Stokes solver. In the wake-induced transitional strip (zone A in Figs. 7 and 8), influence of the velocity defect has the dominant influence. While the turbulence intensity in the wake reaches 10%, the phase lag between k in the freestream and k in the boundary layer reduces the influence of the increased turbulent kinetic energy at this location. An opposite effect is felt in region B, which is located between wake paths. The amplification of the unsteady turbulence near the leading edge leads to an increased level of k from 10 to 30% of the chord. Additional diffusion of the turbulence from the freestream results in a smoother transition, as seen along line Z in Fig. 8.

One of the characteristic features of the unsteady boundary layer is the phase lag between the velocity at the edge and inside the boundary layer. The distance between path I and path II (Fig. 7) is widening with the development of the boundary layer downstream of the leading edge, which is an indication of an increased phase lag in the velocity field. The amplitude and the phase angle of velocity fluctuations are shown in Fig. 9. This phase lag increases from about 30 deg at $X_c/C = 0.4$ to 100 deg at $X_c/C = 0.76$ (Fig. 9b). The predicted phase angle and the amplitude of the first harmonic of the total velocity correlate well with the predictions from the boundary-layer code; this is one of the most important and critical steps in the validation of the Navier–Stokes code. With proper control of the artificial dissipation, grid, and time step, the Navier–Stokes code can be used to predict the unsteady transitional boundary layer accurately.

The predicted momentum thickness, shown in Fig. 10, reveals excellent agreement with the experimental data and the Euler/boundary-layer prediction. Similar to the boundary-layer solution, the Navier–Stokes solver predicts a higher level of time-averaged momentum thickness in comparison with the steady-state solution, which is an indication of an increased loss because of the unsteady interaction. According to the flow visualization, the flow separation occurs near 90% chord. The main drawback of the boundary-layer approach is its inability to simulate the separated flow. The Navier–Stokes code correctly predicts the separation zone, existing from 87% of chord. The predicted separation has an unsteady character; flow conditions vary from the fully attached to the separated flow. A sharp increase in the momentum thickness

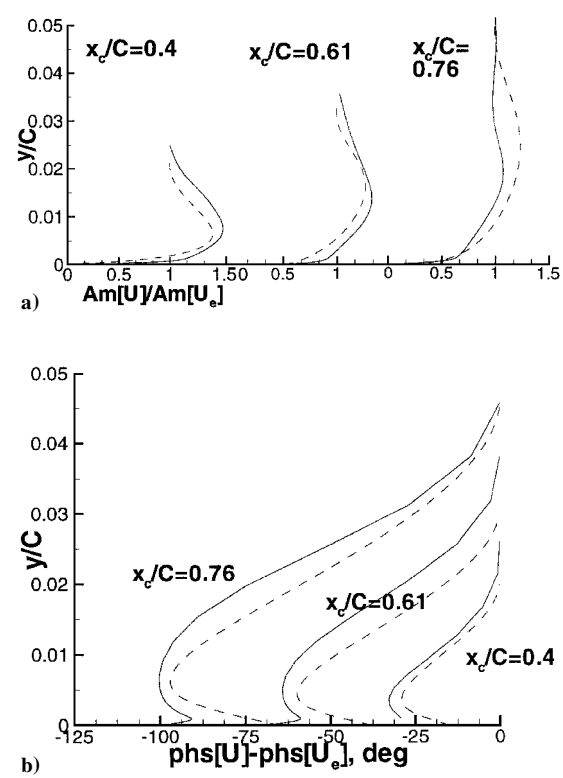

Fig. 9 Velocity profile: a) amplitude and b) phase lag; ——, N–S simulation, and – – – · , boundary-layer simulation.

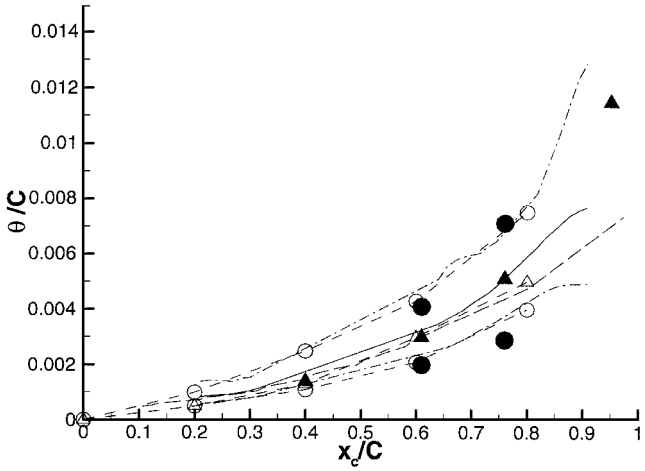

Fig. 10 Momentum thickness, suction surface: ▲, experiment, time average; ●, experiment, min/max; – – –, N–S simulation, steady; ——, N–S simulation, time average; – · –, N–S simulation, min/max; △, boundary-layer simulation, time average; and ○, boundary-layer simulation, min/max.

beyond 85% of chord is because of an earlier separation caused by the passing wake.

Conclusion

An existing steady Navier–Stokes code is extended to include pseudo time stepping, which provided acceleration from 5 to 25 times that of the original code. A systematic validation procedure is implemented to assess the effects of the grid density, the artificial dissipation, and the physical and pseudo time steps for accurate prediction of transitional flows resulting from the rotor-stator interaction.

The ability of the Navier–Stokes code to predict the unsteady transitional flow on a turbomachinery blade is demonstrated. The unsteady pressure and velocity fields are in good agreement with the experimental data and the prediction from the Euler/boundary-layer approach. The numerical solver is able to capture major zones (wake-induced transitional strip, wake-induced turbulent strip, etc.) associated with the wake-induced transition in a compressor cascade.

Another significant step is the assessment of k-ε turbulence models, including leading-edge modifications. The best results are obtained using the FLB model. The LB model predicts earlier inception of the transition and shorter transition length. Modification of the k-ε model is found to be essential for the accurate prediction of the unsteady transitional flow in the compressor cascade. The CH model fails to predict the unsteady transitional flow. The predicted boundary layer is turbulent from the leading edge, even with the modification of the k-ε model near the stagnation point.

The Navier–Stokes simulation requires only two to three times more CPU time in comparison with the Euler simulation if the surface pressure distribution is of primary concern. Thus, the Navier–Stokes solver can be used as a replacement for the Euler code in a coupled Euler/boundary-layer procedure, and so this will combine the efficiency and the accuracy of the unsteady boundary code with the ability of the Navier–Stokes code to predict more accurate pressure distribution, upstream wake decay, off design, and separated flow. The required CPU time in this case is about three times the CPU time required for the original Euler/boundary-layer solver.

Acknowledgments

This work was partially supported by NASA Grant NAG 3-2025, with D. Ashpis as the Technical Monitor. The authors wish to acknowledge NAS at NASA Ames Research Center for providing the supercomputer resources.

References

[1]Fan, S., and Lakshminarayana, B., "On the Prediction of Wake Generated Unsteady Pressure and Boundary Layers in Turbomachinery Cascades," *Journal of Turbomachinery*, Vol. 118, No. 1, 1996, pp. 96–122.

[2]Kunz, R., and Lakshminarayana, B., "Three-Dimensional Navier–Stokes Computations of Turbomachinery Flows Using an Explicit Numerical Procedure and a Coupled k-ε Turbulence Model," *Journal of Turbomachinery*, Vol. 114, No. 3, 1992, p. 627.

[3]Chien, K-Y., "Predictions of Channel and Boundary-Layer Flows with a Low-Reynolds-Number Turbulence Model," *AIAA Journal*, Vol. 20, No. 1, 1982, pp. 33–38.

[4]Lam, C. K. G., and Bremhorst, K., "A Modified Form of the k-ε Model for Predicting Wall Turbulence," *Journal of Fluids Engineering*, Vol. 103, No. 3, 1981, pp. 456–460.

[5]Fan, S., Lakshminarayana, B., and Barnett, M., "Low-Reynolds-Number k-ε Model for Unsteady Turbulent Boundary-Layer Flows," *AIAA Journal*, Vol. 31, No. 10, 1993, pp. 1777–1784.

[6]Arnone, A., Liou, M.-S., and Povinelly, L. A., "Integration of Navier–Stokes Equation Using Dual Time Stepping and Multigrid Method," *AIAA Journal*, Vol. 33, No. 6, 1995, pp. 985–990.

[7]Weiss, J. M., and Smith, W. A., "Preconditioning Applied to Variable and Constant Density Flows," *AIAA Journal*, Vol. 33, No. 11, 1995, pp. 2050–2057.

[8]Melson, L. D., Sanetrik, M. D., and Atkins, H. L., "Time-Accurate Navier–Stokes Calculations with Multigrid Acceleration," Sixth Conf. on Multigrid, N 94-21469, Copper Mountain, CO, April 1993.

[9]Chernobrovkin, A., and Lakshminarayana, B., "Development and Validation of Navier–Stokes Procedure for Turbomachinery Unsteady Flow," AIAA Paper 97-3281, July 1997.

[10]Chevray, R., and Kovasznay, L. S. G., "Turbulence Measurements in the Wake of a Thin Flat Plate," *AIAA Journal*, Vol. 7, No. 8, 1969, pp. 1641–1643.

[11]Savill, A. M., "Synthesis of T3 Case Prediction," *Numerical Simulation of Unsteady Flows and Transition to Turbulence*, Cambridge Univ. Press, Cambridge, England, UK, 1992, pp. 404–443.

[12]Abu-Ghannam, B. J., and Shaw, R., "Natural Transition of Boundary Layers—The Effects of Turbulence, Pressure Gradient and Flow History," *Journal of Mechanical Engineering Science*, Vol. 22, No. 5, 1980, pp. 213–228.

[13]Launder, B. E., and Spalding, D. E., "The Numerical Computation of Turbulent Flows," *Computer Methods in Applied Mechanics and Engineering*, Vol. 3, 1974, pp. 269–289.

[14]Strahle, W. C., Sigman, R. K., and Meyer, W. L., "Stagnating Turbulent Flows," *AIAA Journal*, Vol. 25, No. 8, 1987, pp. 1071–1077.

[15]Schulz, H. D., Gallus, H. E., and Lakshminarayana, B., "Three-Dimensional Separated Flow Field in the Endwall Region of an Annual Compressor Cascade in the Presence of Rotor-Stator Interaction," *Journal of Turbomachinery*, Vol. 112, No. 4, 1990, pp. 669–690.

[16]Halstead, D. E., Wilsler, D, C., Okiishi, T. H., Walker, G. J., Hodson, H. P., and Shin, H.-W., "Boundary Layer Development in Axial Compressors and Turbines," *Journal of Turbomachinery*, Vol. 119, No. 1, 1997, pp. 114–127.

P. R. Bandyopadhyay
Associate Editor